Meteorologisches Institut
Universität Bonn

National Center for Atmospheric Reasearch
Boulder Colorado

Masterthesis

Evaluation of the COSMO- and WRF-Model by Application of the Initial Tendency Method

Florian Losch

30th September 2017

Mentors: Dr. Petra Friederichs and Dr. Judith Berner

Contents

1 Motivation

1.1 Motivation

Correct understanding and prediction of the atmosphere as a dynamical system is important for all societies. While understanding weather and climate has long been the endeavor of many physicist, useful predictions over several days have only been feasible since the advent of electronic computers. Since then the meteorological research as well as private companies have always tried to utilize the growing availability of computation power at the best efficiency.

The scientifically established way of developing models consists of three steps:

- Observe nature, if possible quantitatively.
- Formulate a model describing the observed system, that can also produce verifiable forecasts.
- Make a forecast and then verify the described model

This work concentrates on the third of these steps. There are multiple ways to verify Numerical Weather Prediction (*NWP*) models. Here it is sought to verify the forecasts made by two different models (COSMO and WRF) without gathering of new, independent measurements. While incorporating independent measurements into the verification process allows for additional insight to be found, gathering data not used in the model already can be complicated.

The verification method used here (*Initial Tendency Method*) utilizes independent physical insights that the model has to obey, but that are not guaranteed directly in the model setup. Therefore this method is similar to an investigation of analysis increments.

In contrast to the analysis increments method the Initial Tendency Method will potentially utilize less computational resources and also allow for an analysis of the temporal development of errors, particularly the discrimination between spin-up and constant errors.

2 Theory

2.1 Numerical Weather Prediction Model

Modern weather prediction is based on the use of output from Numerical Weather Prediction (*NWP*) models. First, the procedure of a NWP-model will be described. (Grandy Jr, 2004)

To initialize the numerical model, information about the current state of the atmosphere (and other modelled systems) is needed. These initial values have to be given in the „model space“ , i.e. the state of all variables describing the system are needed at each grid point.

Since it is impossible to measure the state of the atmosphere at each grid point multiple times a day, the process of *d*ata assimilation is used to combine the first guess state of the model with observations.

2.2 Data Assimilation

The main objective of the data assimilation process is to find a model state, that is as close as possible to the observations. A problem addressed by the data assimilation process is the presence of measurement errors. Already small errors in a single measurement can imply extensive imbalances and thereby erroneous processes in the forecast. Therefore it is important to balance the influence of any single measurement with general balance requirements to produce a dynamically consistent initial condition.

The model first-guess state for a particular time is chosen as a single or ensemble forecast with short forecast lead-time. This first-guess state is combined with the observations valid at this time to produce an analysis. The model state is adjusted to reflect the observations, but remains dynamically consistent. This step is called the data-assimilation step. The details on how first-guess state and observations are combined, depends on the specific data assimilation scheme chosen.

2.2.1 Observation Nudging (COSMO)

One particular assimilation scheme is the *observation-nudging*. This scheme is used in the COSMO-model. In this scheme the adjustement is realized by changing the prognostic tendency produced from the model in such a way, that the new state is closer to the observed state. The change for any observed variable $\phi(x,t)$ by kth observation is given by (C. Schraff and Hess, n.d.):

$$\frac{\partial}{\partial t}\phi(\mathbf{x},t) = F(\phi,\mathbf{x},t) + G_\phi \cdot \sum_{k_{(obs)}} W_k(\mathbf{x},t) \cdot \left[\phi_k^{obs} - \phi(x_k,t)\right] \tag{2.1}$$

where F is the tendency produced by model dynamics and physics, G a variable dependent constant, W_k an observation dependent weight decreasing with distance from the observation in space and time and ϕ^{obs} the observed value. By this procedure the model is forced to stay close to observed values, where these are available but can develop freely where they are not.

If the model physics and dynamics $F(\cdots)$ were zero, the assimilation terms would produce a exponential convergence of ϕ to ϕ^{obs}. To guarantee that the modeled system is still conform to the physical model, the assimilation term should be small compared to the model physics and dynamics. To ensure this, W_k is being adjusted with the formula:

$$W_k = \frac{w_k + 1}{\sum_j w_j + 1} \cdot w_k \tag{2.2}$$

where the weight w_k is being limited by the utilization of the sum over all influencing weights w_j. An advantage of this method is that measurements can be added flexibly to the assimilation process whenever they become available, while other methods are only able to incorporate additional information at fixed times.

For nudging-based assimilations, the measured „truth“ has to been known in model space (see ϕ in (2.1)). The conversion of satellites' measurements into model space is intricate and time costly, thus no satellite data are being used in data assimilation.

The incorporation of radar-based precipitation measurements needs a special procedure called *latent heat nudging*. (Stephan, Klink, and Schraff, 2008) It would not be effective to assimilate the observed precipitation in regions, where the model is not producing precipitation, since it would just fall out without adjusting the model trajectory. This would prevent the model from producing better forecasts by adjusting the dynamical processes.

To fix the cause of a inaccurate precipitation where visible by precipitation products, latent heat is added or removed at the cloud base. This will then increase or reduce vertical motion in the cloud which in turn will result in an improved precipitation rate.

While the observation-nudging scheme is rather pragmatic in its design, it performs very well in operational weather forecasts, since it is highly adjustable. In addition, the forecasting framework in an operational setting is easy to set up: the model is always in „data assimilation“ mode. In instances, where no observations are available, the model will automatically run free – the second right-hand term in (2.1) will be zero. To alleviate against strong changes in the model forcing when observations become (un-)available there is a temporal adjustment term.

Another advantage of this scheme is that it allows the model during the data-assimilation step to move to its attractor, which minimizes spin-up errors (see section 2.3.3).

2.2.2 Ensemble Kalman Filter (WRF)

The Data Assimilation Research Testbed (*DART*) employs a sequentially adjusted Kalman filter (Bengtsson, Snyder, and Nychka, 2003) which is an extension of the original Kalman Filter.

Under certain assumptions, the Kalman filter is the optimal solution for the data assimilation problem in linear systems. Suppose the probability distribution of the initial conditions is known as well as the observations and their error distribution. The Kalman Filter proceeds in two steps. (Burgers, Jan van Leeuwen, and Evensen, 1998)

1. A forecast from the initial condition is produced. Because of linearity, the propagation of the uncertainty is feasible computable. The result is called the *B*ayesian prior.
2. Utilizing Bayes' Theorem, the observations and their error distribution are combined with the prior to produce the so called *B*ayesian posterior. This is the data assimilation step.

A new forecast is started from the posterior which is then used as the prior in the next iteration. Due to the repeated iterations of steps 1 and 2, this data assimilation method is also referred to as “cycled”. Cycling allows the assimilation to converge onto the model's attractor, minimizing spin-up. For systems with Gaussian error distributions, this scheme can be shown to produce the optimal solution. (Kalman et al., 1960)

The equations solved by numerical weather prediction however, are strongly nonlinear. This makes it infeasible to predict the propagation of uncertainty with time as the Fokker-Planck equations would have to be solved. The usage of the Ensemble Kalman Filter overcomes this limitation at the cost of losing the optimality of the solution.

The Ensemble Kalman Filter utilizes a bootstrapping method to simulate a solution of the Fokker-Planck equations. To achieve this, the initial uncertainty is represented by an ensemble of initial conditions. To maximize the divergence of the trajectories, the distribution of the initial conditions is chosen to have maximal variance in the directions of the Lyapunov vectors with biggest Lyapunov exponents.

2.3 Forecast Error

From a perspective of model development there are three kinds contributors to forecast error:

- Initial condition error
- Boundary condition error
- Model error

While these sources of error are conceptually different, they are extremely hard to disentangle in practical applications. Even if a model could be perfectly initialized, the model error would lead to a different state after a single timestep. This would result in a different trajectory for this forecast. This is the focus of the article by Judd et al., 2008. Judd describes different types of errors by their origin, neglecting whether they're distinguishable later. He also describes the data assimilation process not as independent, but as part of the model. In the following the different sources of forecast error are further discussed.

2.3.1 Initialization Error

One widely known source of error is flaw in the initial data. Often it is assumed, that uncertainty of the initial state will grow even in a perfect model exponentially with time. Smith, Ziehmann, and Fraedrich, 1999 however finds, that this behavior will not always be observed.

In dissipative systems *sometimes* a initialization error will be dissipated and the model trajectory will converge to the real one. However *statistically* the assumption of an exponential error growth due to initialization errors still holds.

A second source of error are uncertainties in parameters, boundary and initial data, and measurement errors. These errors are thought to be countered by data assimilation and ensemble forecasting.

2.3.2 Boundary Condition Error

Another implication of the exponential growth is, that for a certain time after the beginning the errors due to initialization errors will be small compared to other errors. While having little effect on the model in the beginning, errors in the lateral boundary condition, if that is present, can potentially dominate the forecast, once the errors had the time needed to spread throughout the model domain. (Warner, Peterson, and Treadon, 1997)

2.3.3 Model Error

In recent years, increasing focused has been directed toward model error. (Bauer, Thorpe, and Brunet, 2015) First of all approximations and neglections are necessary to express the continuous equations describing atmospheric motion in a discretized manner, so that it can be solved by a numerical model. For operational forecasts, the forecast needs to be computed within a certain timeframe to be faster than the forecasted event takes place.

Another source of errors are implementation errors. This is expressed by differences between the formal „numerical model“ and the model actually implemented by the source code. One example is shown by Williamson, Olson, and Jablonowski, 2009.

A phase space view of model error: diverging trajectories

Both numerical models as the physical climate are describable by a multidimensional attractor (Judd et al., 2008). For the physical climate this attractor implies a recurrence time of $\mathcal{O}(10^{30}\,\text{yrs})$ for which the climate system would return to a similar state. The spatial dimension of this attractor is within the range of $\mathcal{O}\left(10^{5}\ to\ 10^{6}\right)$ and therefor also too big to be imagined or visualized.

It is observed, that numerical weather models will be strongly attracted to an attractor, which might slightly differ from the physical climate attractor. If a difference between the physical and the model attractor exist and the model is through the nature of the assimilation scheme initialized in a state lying on the physical attractor, in the beginning of the simulation the model will move from the physical attractor to the intrinsic attractor of the numerical model, resulting in erroneous tendencies called *spin up*.

While the most distinct model spin up will only last for a few minutes, slow climate subsystems can create spin-up times of several years (Thornton and Rosenbloom, 2005).

For a deeper understanding of model behavior in general it is essential to create a new set of forecasts produced with the same model. For this purpose, the model is started from different initialization states in the past and a forecast for the past is produced.

Spin Up Error

Spin up errors can also occur due to artificial different treatment of the first time steps of numerical modeling. This can be implemented as simplification or by error. Spin-up error error happen in the first timesteps of the model and have a wide range of timescales.

Spin up errors can be reduced by using appropriate data assimilation. To minimize the time model output is influenced by spin up it's important to use the same model system in data assimilation as will be used for simulation. Also model configuration (choice of

parameterizations) has to be equal. Otherwise the spin up process can need more then several days, dominating the whole forecasting time.

2.3.4 Tendency Error

A numerical forecast model might also exhibit systematic errors in tendencies of variables. These are associated with a timescales of a few hours or so and are often called *f*ast-physics errors.

This kind of error differs from spin up as tendency errors don't diminish with longer forecast periods letting the actual error grow larger and larger.

Integrating a continual tendency error over an increasing timeframe implies a breaking of conservation laws of energy or their transport. These errors are either included by mistake or by neglection of processes in the atmosphere. Examples for such processes might be aerosols, horizontal radiation scattering or sound waves.

Weather forecast models with higher resolution are typically not integrated for more than few days. Therefore small tendency errors might not grow large or appear to be indistinguishable from spin up effects.

2.4 Reforecasts

In NWP centers, the model is frequently updated to fix error in the model. Hence when analysis produced by operational centers are evaluated over long verification periods, they were produced by different versions of the model, which greatly complicates the evaluation process.

For a deeper understanding of model behavior it is essential to create a new set of forecasts produced with the same model. For this purpose, the model is started from different initialization states in the past and a forecast for the past is produced. This forecasts are also referred to as *reforecasts*. This method differs from a reanalysis in that no measurements are incorporated into the forecast.

By freezing on a specific model configuration and re-evaluation of free forecasts from reanalysis initial data, one can investigate the attractor of the numerical model.

There are different applications imaginable for utilizing reforecasts for model evaluation. Remund, Perez, and Lorenz, 2008 compared the model output to measurements and Del Genio and Wu, 2010 investigated physical properties of the climate exhibited by the model in terms of humidity fluxes.

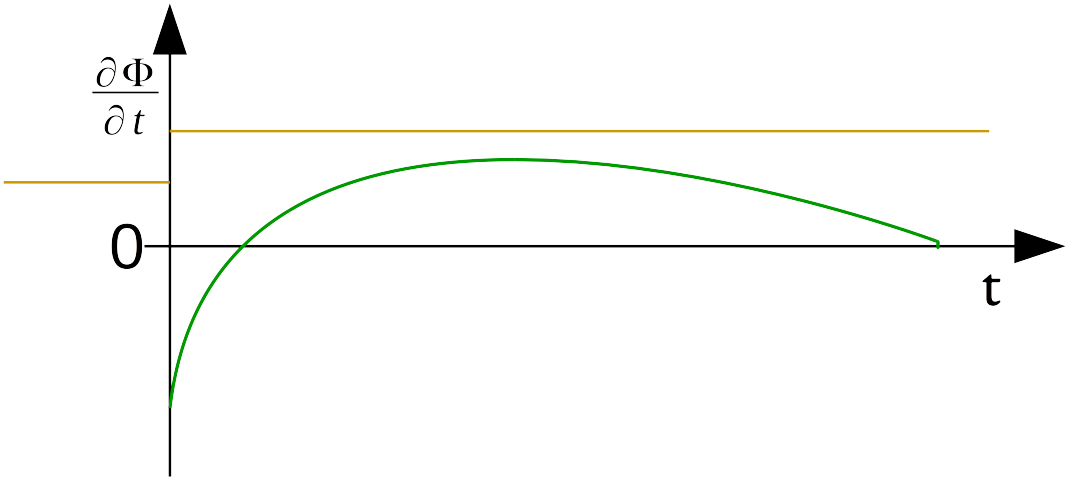

Figure 2.1: *Schematic sketch of the Initial Tendency Method and background tendencies.* The green line shows the corrected tendency $\dot{\Phi}_i$. The orange line shows $\dot{\Phi}^R$, changing at each model start.

Objective of the evaluation method used in this work is to evaluate the models without the use of additional measurements following Rodwell and Palmer, 2007. This kind of evaluation has to verify intrinsic physical properties or the general behavior of the model.

Under the assumption of a stationary climate one can assume, that statistically all variables have to be constant. This is expectable true for extensive or intensive variables.

The time scales for which different variables in the climate system are quasi constant can become very large. Also variables that vary with the diurnal cycle would cause problems, if the diurnal cycle isn't resolved by the model starting times. If the model is for example only started at the local morning, the tendencies for temperature would always be positive whereas this doesn't point to erroneous behavior of the model. It is important to note that the diurnal cycle will sometimes not be resolved by a 6-horal sampling.

Rodwell and Palmer, 2007 are only interested in the model spin-up error, not all model error in general. Therefore, they can solve the problem of separating true error and the diurnal cycle by looking at the difference between the first timestep and the timestep 24 h later.

Due to this for this evaluation known tendencies of all variables will be subtracted before averaging. To determine the known tendencies the reanalysis from which the model is started are used to calculate the real background tendencies, that manifest the model error (the analysis increment) only.

2.5 Initial Tendency Method

For a Variable Φ let Φ_0^R be the reanalysis field from which the model is started and Φ_1^R the next reanalysis field available after a time of ΔT.

The forecast field for t seconds after Φ_0^R is denoted $\Phi^M(t)$. The model time step numbered $0 \leq i \leq n \in \mathbb{N}$ is Δt seconds. Therefore model fields are available for $t = i\Delta t$ and called Φ_i^M.

The Background tendency is $\dot{\Phi}^R = {}^{(\Phi_1^R - \Phi_0^R)}/_{\Delta T}$ if $i < {}^{\Delta T}/_{\Delta t}$, else-wise $\Phi_{2,3,\ldots}^R$ will be used such that the time step i is in between the used reanalysis. The model tendency $\dot{\Phi}_i$ exclusive the background tendency between the time steps i and $i+1$ is then calculated by:

$$\dot{\Phi}_i = \frac{\Phi_{i+1}^M - \Phi_i^M}{\Delta t} - \dot{\Phi}^R \tag{2.3}$$

Occasionally due to practical reasons some model tendencies $\dot{\Phi}_i$ to $\dot{\Phi}_j$ will be examined only averaged:

$$\dot{\Phi}_{ij} = \frac{1}{j-i} \sum_{k=i}^{j-1} \dot{\Phi}_k = \frac{\Phi_j^M - \Phi_i^M}{(j-i)\Delta t} - \dot{\Phi}^R \quad \text{with:} \quad i < j \leq n \tag{2.4}$$

For some variables the model can be configured or adapted to add different tendency terms, that are normally are integrated, directly to the model output. This then allows for another way to compute $\dot{\Phi}_i$:

$$\dot{\Phi}_i + \dot{\Phi}^R = \sum_k \dot{\varphi}_k^M \tag{2.5}$$

Here $\dot{\varphi}_k^M$ are the different model tendencies from the dynamics and physics of the NWP. It is important that all processes are included for this equation to hold.

2.6 COSMO Model

This model is developed mainly by the German weather service (DWD) in cooperation with other institutions in the COSMO consortium. The principle of the development of the COSMO model is operational weather forecasting while research applications are only included where they do not impair operational usability of the model. Here the model is evaluated in a configuration that is as close as possible to DWD's operational configuration.

2.6.1 Coordinate System

Horizontal

The COSMO model utilizes the geographical coordinate system. Following Zdunkowski and Bott, 2003 all terms in the dynamic core emerging from the metric tensor are considered with following simplifications. (Günther Doms and Baldauf, 2011, p.20ff)

- Gravitational acceleration is assumed to be constant
- Where the total radius is needed, height over the surface is neglected.
  - This renders the curvature of all model levels independent of height.
  - For consistency Coriolis acceleration on and due to vertical motion has to be neglected
- The coordinate north pole is rotated away from the true north pole such that the coordinate equator runs through Europe. This minimizes numerical errors due to the coordinate system but complicates the Coriolis acceleration.
- Where the total radius is needed, height over the surface is neglected.
  - This renders the curvature of all model levels independent of height.
  - For consistency Coriolis acceleration on and due to vertical motion has to be neglected

Vertical

Using constant height or pressure as a vertical coordinate is not feasible, because the resulting model layers would intersect with orography at the lower boundary. Atmospheric flows also follow the orography strongly in the lower atmosphere. Additionally a higher resolution of vertical atmospheric movement is desirable in the lower layers compared with the upper atmosphere.

- The vertical structure should follow the orography closely where it is close.
- The layers should be smoother in the upper atmosphere.
- The vertical resolution should increase towards the lower boundary.

For the vertical structure the *Height-based hybrid SLEVE coordinates* are being used in the COSMO model. They provide exponential vertical smoothing of the orography and are not pressure dependent but height based.

In the model configuration the vertical levels are initialized in such a way, that the differences of their mean height decreases exponentially towards the ground in the lower 6 km and are constant above that. (Günther Doms and Baldauf, 2011, p.31ff)

2.6.2 Sound Waves

To allow for stability even on grid point distances that can also feature sound waves, time resolution has to be increased to resolve those waves. Due to the high speed of sound, the time resolution has to be increased up to 8-fold. (Günther Doms and Baldauf, 2011, p.133ff) To enable both the resolvability of sound waves as well as practical performance of the model the numerical timestepping is complicated. During most timesteps („fast timesteps“)only those terms are updated that are needed to resolve sound waves. Here the numerical accuracy and stability is also reduced in favor of better performance, and the terms of the parameterizations are not updated at all (assumed constant). During the „regular timesteps“ the numerical accuracy in the dynamic core of the model is higher and some parameterizations are updated. Other parameterizations like the radiation are not decided to be updated at even every „regular timesteps“ given their high complexity and impact on the performance.

2.7 WRF Model

In contrast to the COSMO model the WRF model is published under a public domain license. While the National Center for Atmospheric Research (NCAR) has trademark protection on the name and is leading the development of the model, everyone is free to download the source code, modify it and redistribute it freely as long as the re-publishment is still in public domain. (NCAR, 2012)

2.7.1 Coordinate System

Horizontal

As WRF's dynamic core does not implement metric terms (Skamarock and Klemp, 2008), the choice of the coordinate system is of high importance. In these simulations the *Lambert conformal projection* was chosen for the horizontal coordinates. (Lambert, 1772) The *Lambert conformal projection* is mainly used in aeronautics due to it's property that the shortest path between two points on the sphere is a straight line, without losing conformity. To allow for both qualities, the area of each gridpoint has to be different. Also, the same map cannot simultaneously show two points which are on opposite sides of the sphere.

Vertical

The WRF model uses a terrain-following vertical coordinate similar to the COSMO model following Laprise, 1992. One difference is that here a generalized variable based on hydrostatic pressure is used to identify different heights in the atmosphere. Also, there is no cut-off height at which orography seizes to influence the vertical coordinate.

2.7.2 Sound Waves

Through numerical inaccuracies and accuracy limits of digital floating point number representation there will always be random artificial artifacts in all prognostic fields. These inaccuracies will sometimes lead to imbalances in the pressure field that result in fast artificial sound waves. These sound waves, if correctly modeled, are not relevant for the energy budget or other meteorological variables. In coarser grained, hydrostatic NWPs these inaccuracies can be filtered out after each time step. Here this is not possible. Therefore sound waves need to be modeled correctly. For this the time stepping needs to be significantly increased (about 8-fold). But to run the normal dynamic core at these short time steps would be too inefficient.

Therefore, most timesteps are reduced in numerical precision to the point where only sound waves are modeled accurately enough such that no instabilities arise, while the full-accuracy numerics remain at the slower speed, comparable to hydrostatic models. (Skamarock and Klemp, 2008)

3 Methodology

3.1 Entropy Production

3.1.1 Entropy Temperature

To calculate according to Hauf and Höller, 1987

$$\text{mixing ratio: } r^t = r^1 + r^2 + r^3$$

$$c^* = c_{p0} + c_2 r^t$$

$$a_{21} = R_1 T \ln \frac{p^{21}}{p^1}$$

$$a_{32} = R_1 T \ln \frac{p^{31}}{p^{21}}$$

$$\Theta_s = T\left(\frac{p^0}{p_0}\right)^{-\frac{R_0}{c^*}} \cdot \exp\left[\frac{(l_{21}+a_{21})r^1}{c^* T} - \frac{(l_{32}+a_{32})r^3}{c^* T}\right] \tag{3.1}$$

3.1.2 Entropy Production

$$\frac{\mathrm{d}s}{\mathrm{d}t} = m^0 c^* \frac{\mathrm{d}\ln\Theta_s}{\mathrm{d}t} \tag{3.2}$$

3.2 Richardson Number

$$\text{Brunt-Väisälä frequency: } N = \sqrt{\frac{g}{\Theta}\frac{\mathrm{d}\Theta}{\mathrm{d}z}}$$

$$Ri = \frac{N^2}{\left(\frac{\mathrm{d}u}{\mathrm{d}z}\right)^2} \tag{3.3}$$

3.3 COSMO

3.3.1 Model Version and Configuration

The COSMO model is compiled from version 4.28 and used in the same configuration as run by the German Weather Service. The horizontal grid spacing is with 2.8 km convection permitting. The modeled region is Germany (*COSMO_DE*). The initial data are taken from the HErZ reanalysis project. (Kneifel et al., 2012) For six days in summer 2011 reforecasts have been initialized twice daily at 12:00 and 14:00 MEST.

3.3.2 Physics Parameterizations

Parameterizations are those parts of the model, that influence the model while only taking into account values at a single column or even grid point, not considering horizontal adcevtion. They calculate the influence processes have on the atmosphere, that are smaller than the resolution of the model will resolve.

Gridscale Precipitation

The water droplets forming precipitation are always smaller than the grid resolution of a weather forecast model. In the COSMO model the precipitation scheme will forecast cloud water, cloud ice, graupel, snow and rain. (Doms, 2011, p.68ff)

Radiation

In the COSMO model the radiation scheme, due to its high complexity, is only updated every every 50 regular timesteps (15 minutes). The horizontal resolution is also reduced. In the scheme only the vertical radiative fluxes are calculated while the horizontal fluxes are neglected. To calculate these fluxes water and ice content at grid- and sub-grid scale are used from the model's default diagnostic scheme.

Aerosols are not modelled in this setup of COSMO and their distribution is assumed constant in the radiative scheme. To determine the surface albedo the general soil type is used. (Doms, 2011, p.90ff)

Convection

The original Tiedtke scheme was developed to remove all thermic instability from the model, modelling „deep convection“ . In this model some atmospheric instabilities will also be removed by processes modelled by the dynamic core. The convection scheme therefor has to be adapted. (Doms, 2011, p.80ff)

Here only „shallow convection“ is parameterized, by allowing the Tiedtke scheme to only move latent heat between adjacent vertical layers. Convective tendencies are updated every 10 timesteps (3 minutes) at full horizontal resolution. This shallow convection scheme does therefore not not allow for a CAPE or TKE closure.

Vertical turbulent diffusion

To calculate vertical turbulent diffusion (not resolved by the dynamic core), in this setup a prognostic TKE-based (*Turbulen Kinetic Energy*) is used. As a big driver of sub-gridscale diffusion latent heat is an important part of the scheme. It includes effects from subgrid-scale condensation/evaporation and water from grid- and sub-gridscale water clouds. At the lower boundary, boundary conditions for heat and moisture are in Neumann-form (in terms of W/m^2). (Doms, 2011, p.16ff)

Soil Processes

To estimate the heat fluxes from the lower boundary it is necessary to model some processes inside the soil. Here the available *FLake* (Doms, 2011, p.130ff) model is not used for lakes, but lakes are treated like a special soil type. For heat fluxes in the soil *TERRA* is run with seven distinct soil layers. (Doms, 2011, p.107ff)

The water content in the soil is tracked in two soil-water-layers. To model the heat conductivity an average soil moisture is used. For transpiration effects of vegetation and bare soil the *BATS* model is used without a minimum stomata resistance map.

3.3.3 Initialization

The initial data used from the HeRZ-reanalyses (Kneifel et al., 2012) are in this work considered as free from systematic biases. With this assumption no errors can be found, that are not constrainable by measurements during data assimilation.

3.3.4 Retrieving Tendency Data

To have the model output special variables, that are not pre-configured for output, like the entropy temperature and their tendencies. The *tracer* framework of the model is utilized.

Here the added tracers are configured in such a way that the model will not interact with them in any way automatically. For this advection, diffusion, turbulent mixing, convection and surface fluxes have to be turned off. These configurations take place in the *organize_phyics.f90* file of the source code:

```
CALL trcr_new(                                                    &
ierr          = izerr,                                            &
yshort_name   = 'T_ENTR',                                         &
igribparam    = 52,                                               &
igribtable    = 1,                                                &
yparent       = 'organize_physics',                               &
yunits        = 'kg kg-1',                                        &
ystandard_name = 'entropy_temperature',                           &
ylong_name    = 'entropy temperature after hauf, hoeller 87')!Dont do anything
```

With this the model provides a static numeric field that can be written to at any place during the model run. The entropy temperature is calculated in the source code module *src_gscp.f90*. There, inside the subroutine *hydci_pp_gr* and both the i- and j-loop the following code is added:

```
r1=qvg        !water vapor
r2=qrg+qcg    !rain, cloud water
r3=qig+qsg+qgg !cloud ice, snow, graupel
p1=r1*r_v/r_d*ppg
c_s=cp_d+c_w*(r1+r2+r3)
t_entr(i,j,k)=tg*(((ppg-p1)/100000.)**(-r_d/c_s))* &
         EXP((lh_v+r_v*tg*LOG(fpvsw(tg)/p1))*r1/(c_s*tg)- &
             (lh_f+r_v*tg*LOG(fpvsi(tg)/fpvsw(tg)))*r3/(c_s*tg))
```

With this code added, the model can be configured to add *T_ENTR* containing the entropy temperature to the output which can then be further analyzed.

3.3.5 Background Tendencies

To exclude the background tendencies from the output, the same analysis fields are used from which the model was started.

3.4 WRF

3.4.1 Model Version and Configuration

The WRF model is used at version 3.6.1 in the same configuration as the mesoscale NCAR ensemble. (Schwartz et al., 2015) The outer domain covers the US at a resolution of 15 km. For the WRF model 11 forecasts in ensembles of size 50 in the spring 2015 are analyzed.

3.4.2 Physics Parameterizations

Microphysics

To generate precipitation and model the microphysics of cloud drop and ice formation the *New Thompson* model is used. (Thompson et al., 2008) It models cloud water and ice, rain, snow and graupel as well as number densities for these variables.

Radiation

For long- and shortwave radiation the same *RRTMG* scheme is used. (Iacono et al., 2008) Stochastic cloud overlap is modeled. For long wave radiation it considers the optical depth of clouds and uses pre-computed tables to model absorption and emission through water vapor, CO_2, ozone or other trace gases.

For short wave radiation only downward fluxes are integrated. Any reflected light is assumed to leave the atmosphere. Cloud albedo, cloud absorption, clear-air-scattering and water vapor absorption are taken into account.

Surface Layer

To calculate all needed fluxes at the surface layer the here used *MYJ surface scheme* is based on the Monin-Obukhov similarity theory. Additional corrections are introduced over water surfaces, for vanishing wind speeds and to take into account the effects of viscid boundaries. The computation utilizes an iterative method. (Monin and Obukhov, 1954; Janjić, 1994; Janjić, 1996; Janjić, 2001)

Boundary Layer

For the calculation of turbulent fluxes in the boundary layer the *Mellor-Yamada Level 2.5* turbulence closure model is used. Depending on the shear and buoyancy of the flow in this

implementation an upper limit to the turbulent length scale is introduced. The resulting equations for sinks and sources of turbulent kinetic energy are also solved iteratively. (Janjić, 1994)

Convection

In contrast to the COSMO model, all convective processes have to be parameterized in this configuration of the WRF model, as the grid spacing of 15 km will not resolve any convection directly.

Similar to the COSMO model the *Tiedtke scheme* is used here too. Here however not only shallow but all convection is considered. The Tiedtke scheme allows for representation of various types of convection like deep penetrating clouds, shallow convection or organized convection in unstable conditions. (Tiedtke, 1989; Zhang, Wang, and Hamilton, 2011)

3.4.3 Retrieving Tendency Data

To gather the needed variables from the WRF model, first the used variables are added to the *registry* into a new file. To have all variables available it is needed to add the code to the numerical solvers *solve_em.F* and *module_small_step_em.F*. Here the function calls have to be adapted to contain the new variables:

```
    CALL small_step_prep( ![...]
                          grid%t_tend_dyn, grid%ru_tend_dyn, grid%rv_tend_dyn, &
```

Then before *after_all_rk_steps* is called the following code is inserted to accumulate the tendency component terms.

```
IF ( config_flags%initend ==1) then
!$OMP PARALLEL DO &
!$OMP PRIVATE ( ij ii kk jj )
DO ij = 1 , grid%num_tiles
DO jj = grid%j_start(ij), min(grid%j_end(ij),jde-1)
   DO kk = k_start, min(k_end,kde-1)
      DO ii = grid%i_start(ij), min(grid%i_end(ij),ide-1)
         grid%h_diabatic_acc(ii,kk,jj) = grid%h_diabatic_acc(ii,kk,jj) +
             grid%h_diabatic(ii,kk,jj)
         grid%t_tend_dyn_acc(ii,kk,jj) = grid%t_tend_dyn_acc(ii,kk,jj) +
             grid%t_tend_dyn(ii,kk,jj)/grid%msfty(ii,jj) + &
         grid%t_tendf_diff(ii,kk,jj)/(grid%mu_2(ii,jj)+grid%mub(ii,jj))
         grid%ru_tend_dyn_acc(ii,kk,jj) = grid%ru_tend_dyn_acc(ii,kk,jj) +
             grid%ru_tend_dyn(ii,kk,jj)/grid%msfuy(ii,jj) + &
```

```
        grid%ru_tendf_diff(ii,kk,jj)/(0.5*(grid%mu_2(ii,jj)+grid%mu_2(ii-1,jj) +
            grid%mub(ii,jj)+grid%mub(ii-1,jj)))
        grid%rv_tend_dyn_acc(ii,kk,jj) = grid%rv_tend_dyn_acc(ii,kk,jj) +
            grid%rv_tend_dyn(ii,kk,jj)/grid%msfvx(ii,jj) + &
        grid%rv_tendf_diff(ii,kk,jj)/(0.5*(grid%mu_2(ii,jj)+grid%mu_2(ii,jj-1) +
            grid%mub(ii,jj)+grid%mub(ii,jj-1)))
     ENDDO
   ENDDO
ENDDO
ENDDO
!$OMP END PARALLEL DO
endif
```

To ensure that also all increments during the fast time stepping are included, the *module_small_step_em.F* must also be changed. At the end of the subroutine *small_step_finish* the following code has to be added for the temperature:

```
IF ( initend ==1) then
 t_tend_small(i,k,j)=(t_2(i,k,j)-t_1(i,k,j))/(dts*number_of_small_timesteps)&
                    -(t_tend(i,k,j)/mut(i,j))
 t_tend_large(i,k,j)=(t_tend(i,k,j)/mut(i,j))-(t_tendf(i,k,j)/mut(i,j))
 t_tend_dyn(i,k,j)= t_tend_large(i,k,j)+t_tend_small(i,k,j)
ENDIF
```

3.4.4 Background Tendencies

Background tendencies here are calculated from the same data set, that is used to initialize the model. Here however, in contrast to the COSMO experiment, these fields are available only at 6-horal intervals.

Because of this coarse temporal resolution of the background tendencies an analysis of the first timestep or the temporal development of the tendencies would not be meaningful, as the diurnal cycle would still be part of the tendency and they would therefore not be synonym with model error.

4 Evaluation

4.1 COSMO

4.1.1 Lowest Model Levels

For the COSMO model the first results are the temperature tendencies on each model level. In 4.1 these are shown for the first timestep and averaged over all timesteps respectively. Tendencies in the magnitude of several Kelvins per day are found across the atmosphere. The most distinctive error are the lowest two model levels for the first timestep.

In figure 4.2 for comparison the tendency of the entropy temperature is shown. Here we see the same distinct feature in the lowest two model levels. When all timesteps are looked at, the resulting tendencies become equally positive for the temperature tendency while the entropy temperature shows a dipole. Here the lowest level has a negative tendency while the second level is still positive.

To further investigate these errors the temperature tendency is split up into its constituents from the physics parameterizations. In 4.3 the convective and latent heat parameterization in the first and over all timesteps are shown. Evidently the convective parameterization shows the biggest term in the lowest layer for the first timestep.

In 4.5 the temporal development of the entropy temperature tendency error is shown for different model layers. Here it is visible that while for the first timestep on the lowest level a strongly negative tendency exists, all other tendency errors displayed are positive. Another interesting feature in this plot is the fast change of the tendency in the lowest and second lowest model layer.

Taking these findings together it becomes evident that during the first timestep the model is becoming too cold and dry in the lowest level while it is becoming too hot and moist in the second level. The convective parameterization also behaves in a fitting way, being more strongly active in the first timestep and only weakly active aggregated.

An overly active convective parameterization seems therefore to be causative for the positive temperature error in the lower atmosphere.

4.1.2 Cloud Base

In 4.4 and 4.2 at 2 km a peak positive tendency is visible. At this height the cloudbase is expected to lie. In 4.3 we see that the convective scheme has a maximum here while the latent heat scheme has a minimum above, where the convective parameterization begins to cool the atmosphere.

In 4.5 we also see that the tendency error at 2 km height is unlike the error near the ground not caused by a spin up effect, but comparatively constant over time. Therefore, another error in the model must be present here. Taking the model configuration into account, it seems standing to reason that model dynamics and the convective parameterization generate vertical motion in excess. This problem is known as *convective double counting* and is likely to occur in models that need to parameterize smaller scale convection, while larger scale convection is already resolved by the model's dynamic core.

4.1.3 Vertical Motion

In 4.6 the vertical velocity tendency of different model layers is displayed. It is visible here that most strongly in the higher atmosphere distinctive wave motion is developed. After only a few minutes these waves' amplitude is already significantly reduced. It is reasonable to assume that these artifacts originate from a spin-up effect. As the amplitude converges towards 0 and not some other value, no other error but the spin-up can be found here.

4.2 WRF

4.2.1 Boundary Layer

In 4.15 and 4.16 the components of the temperature tendency and the resulting tendency error are shown. In the lower five model levels a negative tendency of $-1\,\mathrm{K\,d^{-1}}$ is found. The vertical structure of the error term coincides with that of the boundary layer parameterization in 4.15.

In 4.17 the horizontal structure of the temperature tendency error is displayed. Here it becomes evident that the negative (red) tendencies are strongest there, where either a coast or a lake is present in the terrain. It is therefore standing to reason that these topographical features are also causative to the error. One explanation would be an inadequate representation of lake- and sea-breezes through the boundary layer scheme.

Another source of error, that could explain these patterns, lies in the missing representation of any internal dynamics of lakes or the open sea. It is reasonable to assume that these missing dynamics lead to a faulty heating and cooling behavior through the same solar in-

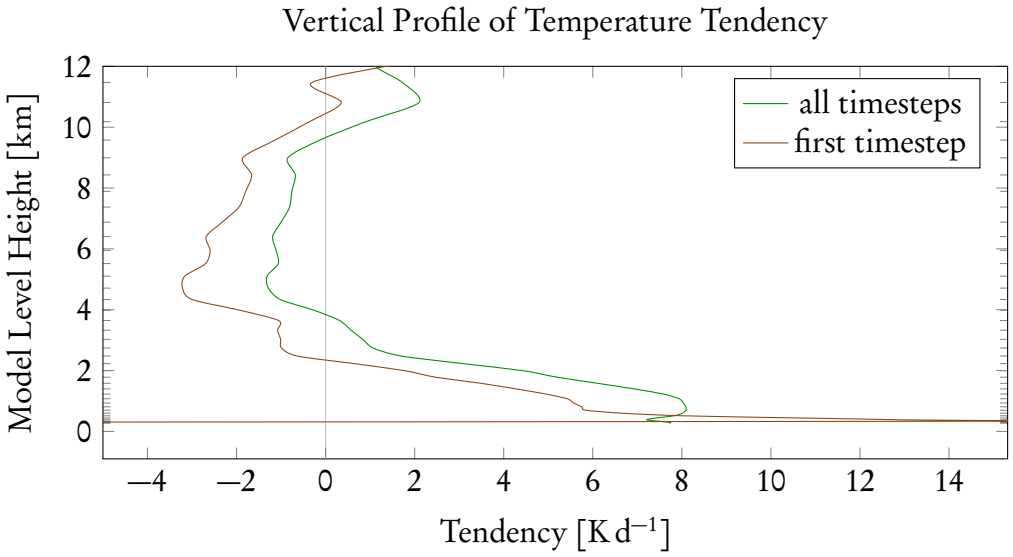

Figure 4.1: *y axis:* For the vertical profile model levels have been used. For each level the mean height is used. Full model levels are taken to be in the geometric mean height between half levels. *x axis:* Tendency of the model Temperature. Using the first timestep only (brown) and the mean for all timesteps (green). Values for the lowest and highest model levels are omitted and $< -20\,\mathrm{K\,d^{-1}}$.

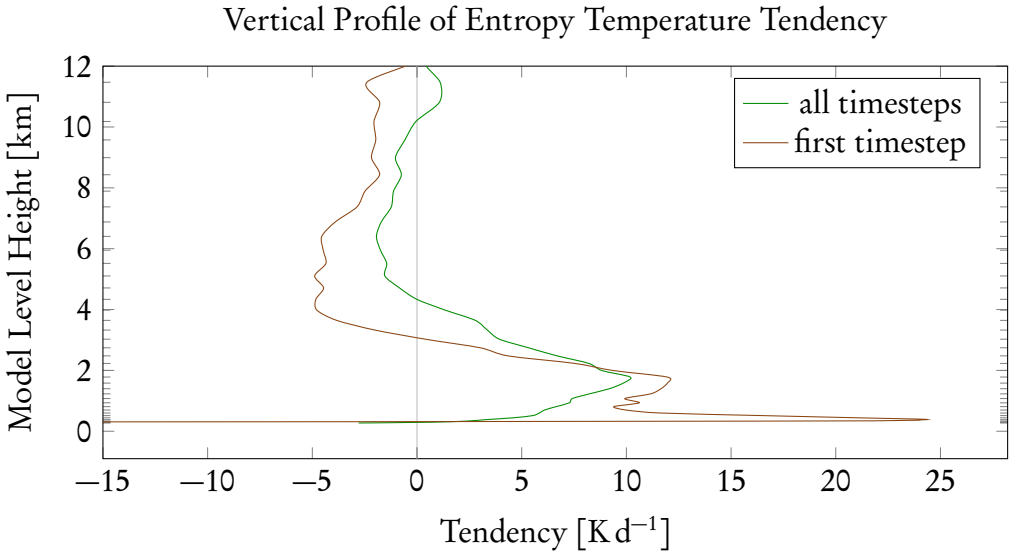

Figure 4.2: *y axis:* For the vertical profile model levels have been used. For each level the mean height is used. Full model levels are taken to be in the geometric mean height between half levels. *x axis:* Tendency of the model Entropy Temperature. Using the first timestep only (brown) and the mean for all timesteps (green). Values for the lowest model levels are omitted and $< -180\,\mathrm{K\,d^{-1}}$.

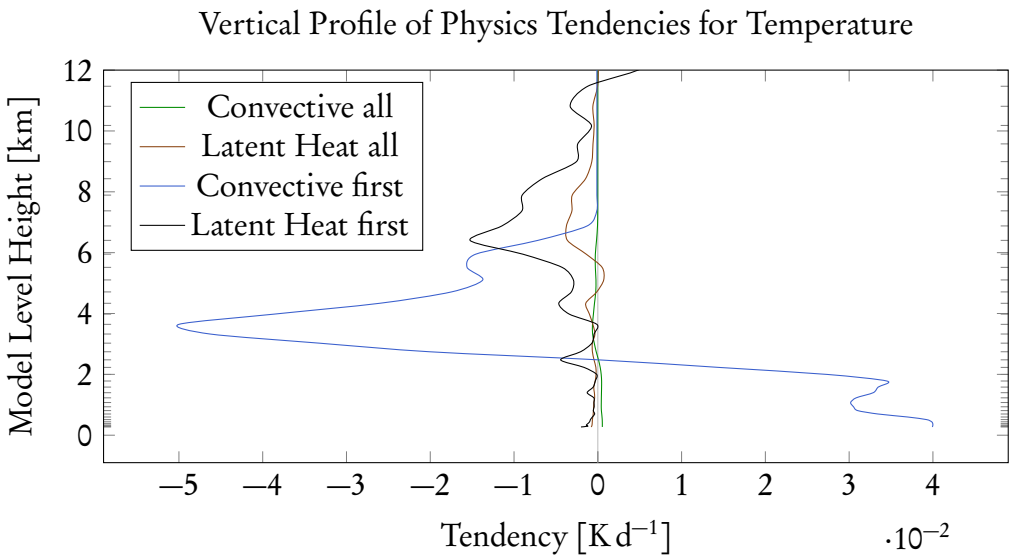

Figure 4.3: *y axis:* For the vertical profile model levels have been used. For each level the mean height is used. Full model levels are taken to be in the geometric mean height between half levels. *x axis:* Constituents of the model temperature tendency. Using the first timestep only and all timesteps and the mean for all timesteps .

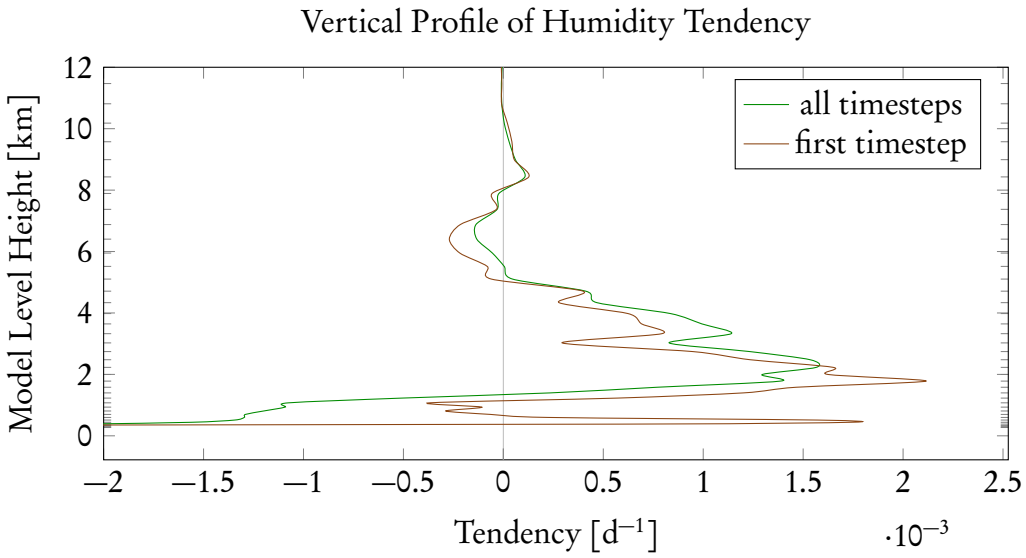

Figure 4.4: *y axis:* For the vertical profile model levels have been used. For each level the mean height is used. Full model levels are taken to be in the geometric mean height between half levels. *x axis:* Tendency of the model Humidity (mixing ratio of water vapor). Using the first timestep only (brown) and the mean for all timesteps (green). Values for the lowest model level are omitted and $< -1.5\,\%\,\mathrm{d}^{-1}$. Values for the upper atmosphere (not shown) are very close to 0.

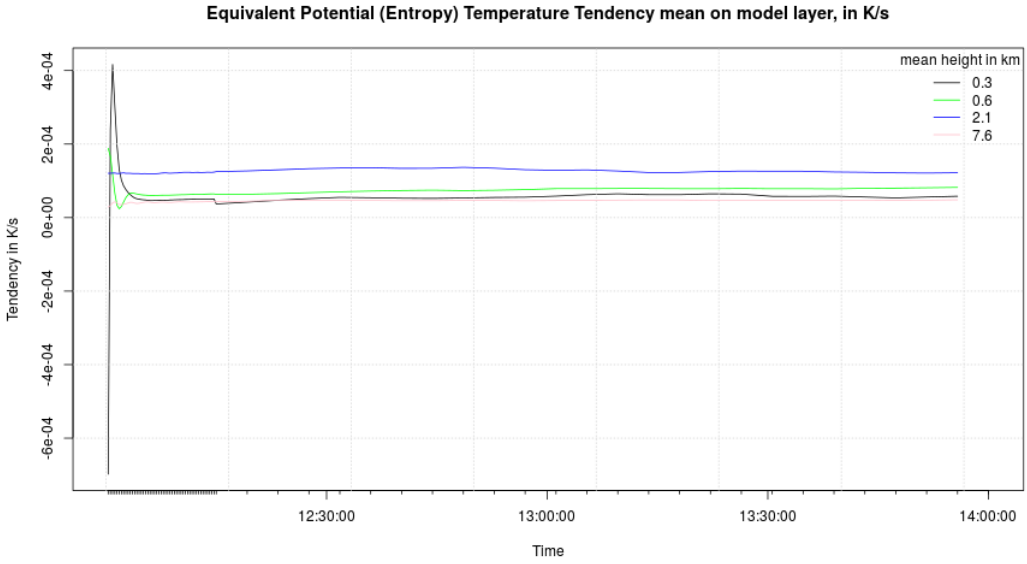

Figure 4.5: Tendency of the entropy temperature on different model levels averaged over all runs from 12:00 to 14:00 MEST. *x axis* Time of forecast, averaged over multiple days. Tickmarks signify the times for which model output was analyzed. *y axis* Tendency exclusive the background tendency for each hour in $\mathrm{K\,s^{-1}}$

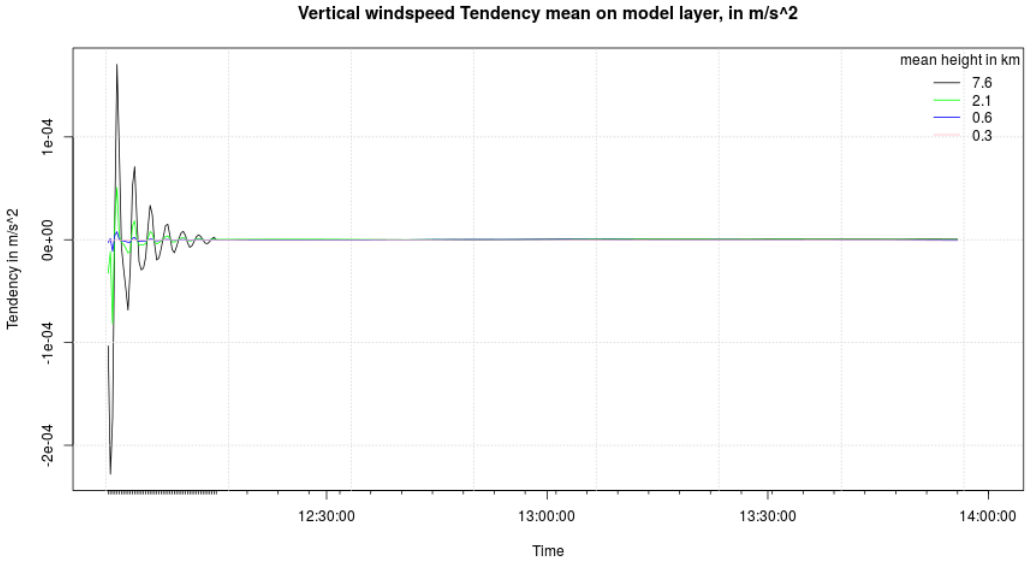

Figure 4.6: Tendency of the vertical velocity on different model levels averaged over all runs from 12:00 to 14:00 MEST. *x axis* Time of forecast, averaged over multiple days. Tickmarks signify the times for which model output was analyzed. *y axis* Tendency exclusive the background tendency for each hour in $\mathrm{m\,s^{-1}}$

put over time. The dynamics of a lake could for example increase the apparent heat capacity depending on the wind. These errors at the ground would then lead to the observed flaw of energy transport by the boundary scheme.

4.2.2 Upper Atmosphere

Another error visible in 4.16 is between level 27 and 31. At level 27 there is a negative temperature bias, which turns positive at level 31 above. As seen in 4.15 this coincides with a decrease of the radiative cooling and an increase of cooling seen in the background tendency.

It is plausible to assume that the decrease of radiative cooling marks the lower boundary of the stratosphere signified through increasing ozone constituents. Considered together with the dipole structure the most natural explanation seems to be an error at the forecasted height of the tropopause.

The height of the tropopause is directly dependent on the height of the ozone layer and sometimes even defined in this way. It is unlikely that the background tendency is influenced by the diurnal cycle at the tropopause. Therefore, it is assumed that the tendency originates from the seasonal cycle.

The model was run during spring in the northern hemisphere. Here it is recognized that the tropopause will ascend. In this model configuration lacking any ozone chemistry representation any change of the height of the tropopause cannot be forecasted. The changes are however added to the model by means of the analysis fields, which causes the background tendency.

4.2.3 Precipitation

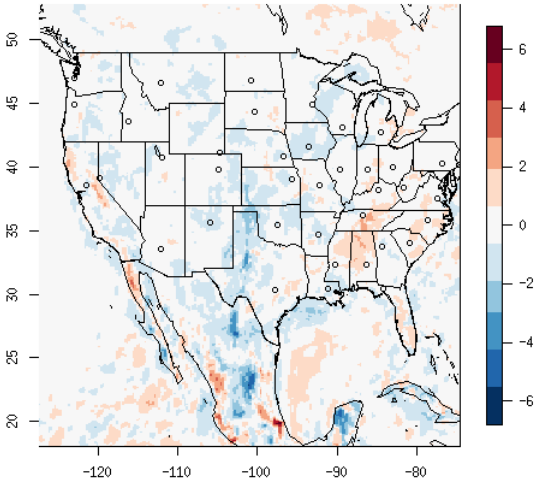

Figure 4.7: *x & y-axis:* Degree North and West, state and country borders are indicated in black lines, state capitals are indicated by black circles *Colors:* The tendencies of the sum of all moisture variables (vapor, liquid and ice) in the lowest 5 model levels in units of $kg\,kg^{-1}\,s^{-1}$.

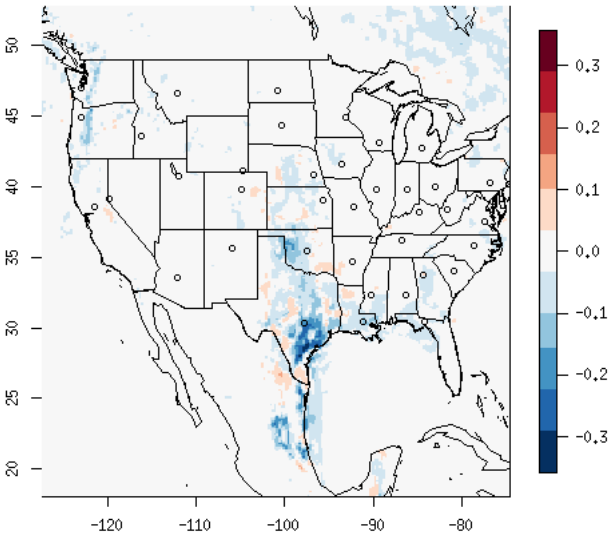

Figure 4.8: *x & y-axis:* Degree North and West, state and country borders are indicated in black lines, state capitals are indicated by black circles *Colors:* The tendencies of cloud water in the model levels number 1 to 5 between 12:00 and 18:00 UTC in units of $kg\,kg^{-1}\,s^{-1}$.

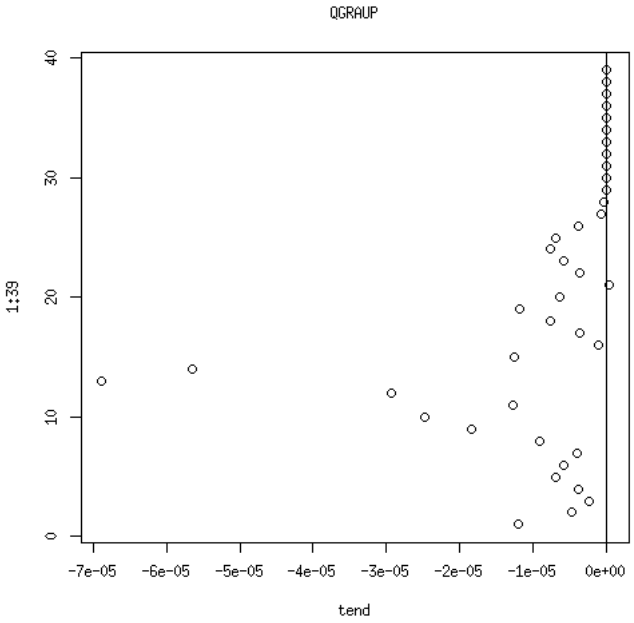

Figure 4.9: *x axis:* Horizontally averaged tendency of the graupel content between 12:00 and 18:00 UTC in units of $\mathrm{kg\,kg^{-1}\,s^{-1}}$. Only values north of the tropics are included. *y axis:* number of the model level.

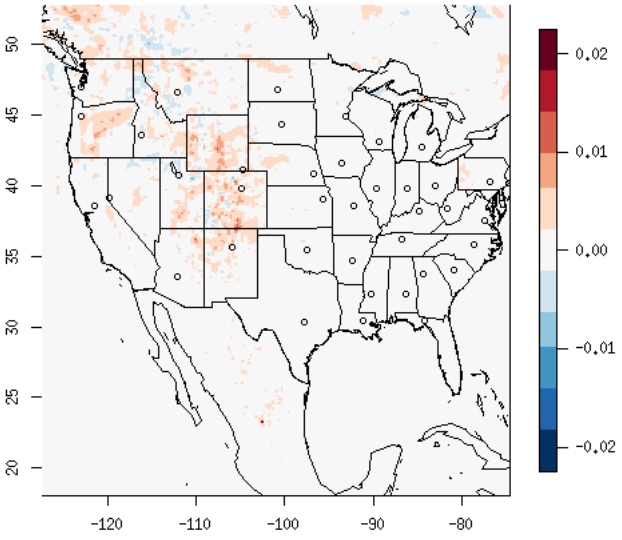

Figure 4.10: *x & y-axis:* Degree North and West, state and country borders are indicated in black lines, state capitals are indicated by black circles *Colors:* The tendencies of cloud ice in the model level number 17 between 12:00 and 18:00 UTC in units of $\mathrm{kg\,kg^{-1}\,s^{-1}}$

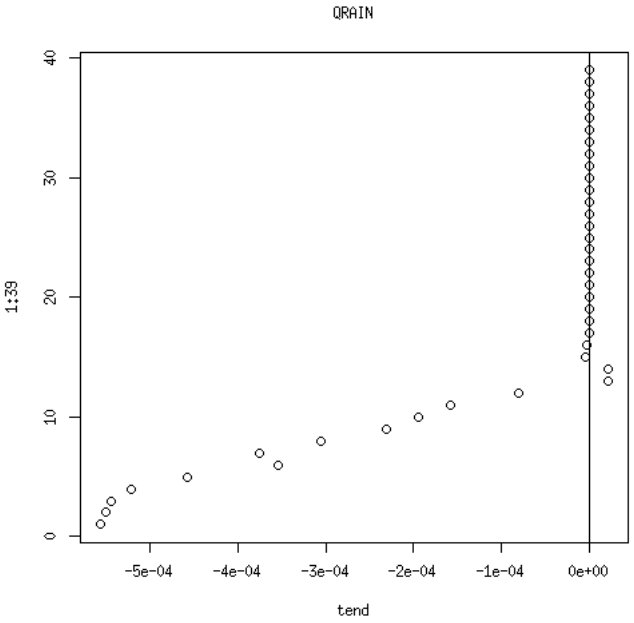

Figure 4.11: *x axis:* Horizontally averaged tendency of the rain content between 12:00 and 18:00 UTC in units of $\mathrm{kg\,s^{-1}}$. Only values north of the tropics are included. *y axis:* Number of the model level.

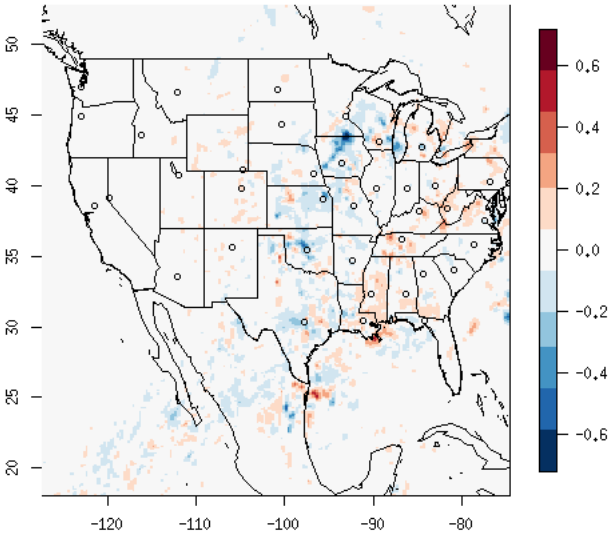

Figure 4.12: *x & y-axis:* Degree North and West, state and country borders are indicated in black lines, state capitals are indicated by black circles *Colors:* The tendencies of snow in the model level number 17 between 12:00 and 18:00 UTC in units of $\mathrm{kg\,kg^{-1}\,s^{-1}}$

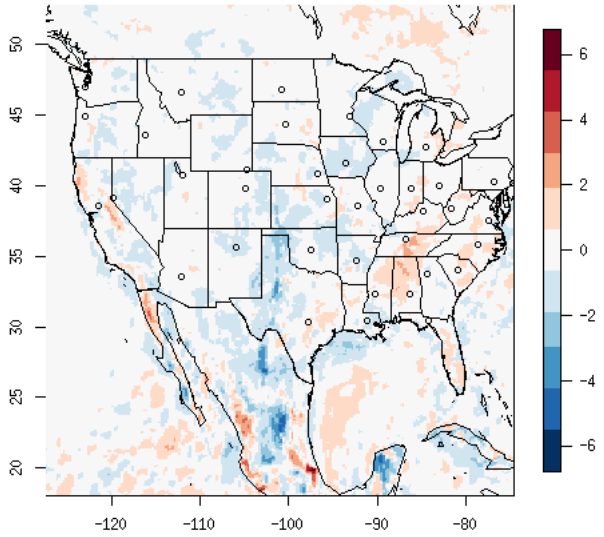

Figure 4.13: *x & y-axis:* Degree North and West, state and country borders are indicated in black lines, state capitals are indicated by black circles *Colors:* The tendencies of water vapor in the model levels number 1 to 5 between 12:00 and 18:00 UTC in units of $\mathrm{kg\,kg^{-1}\,s^{-1}}$

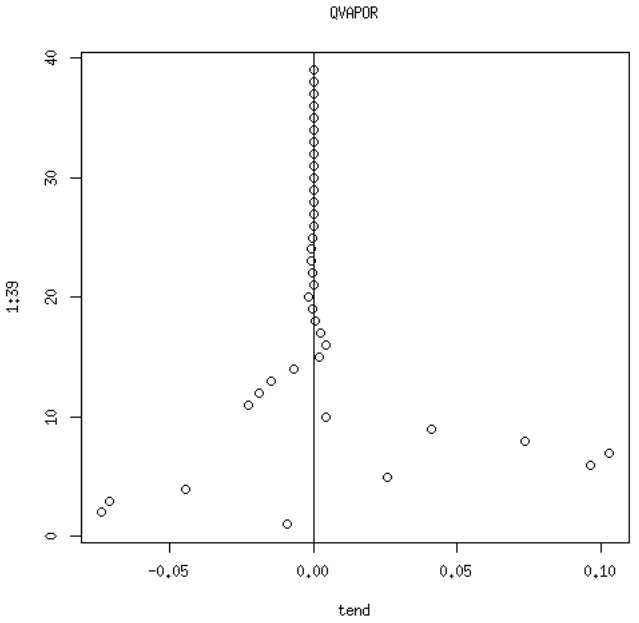

Figure 4.14: *x axis:* Horizontally averaged tendency of the water vapor content between 12:00 and 18:00 UTC in units of $\mathrm{kg\,kg^{-1}\,s^{-1}}$ *y axis:* Number of the model level.

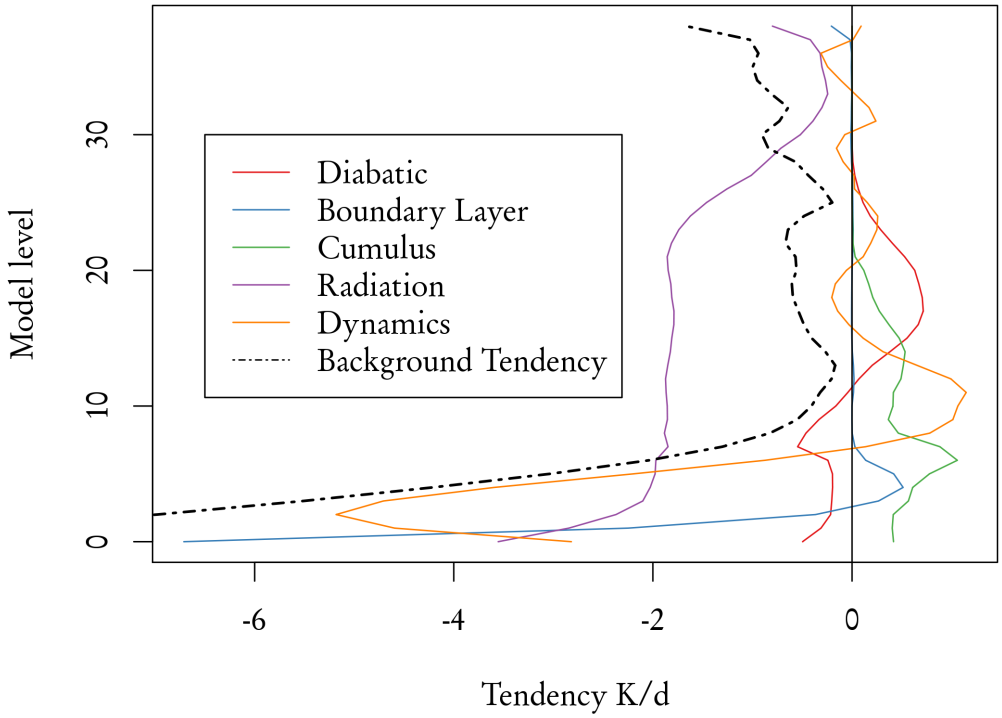

Figure 4.15: *x axis:* Horizontally averaged tendency of the model components for the temperature between 12:00 and 18:00 UTC and background tendency in units of $\mathrm{K\,d^{-1}}$. Only values north of the tropics are included. *y axis:* Number of the model level.

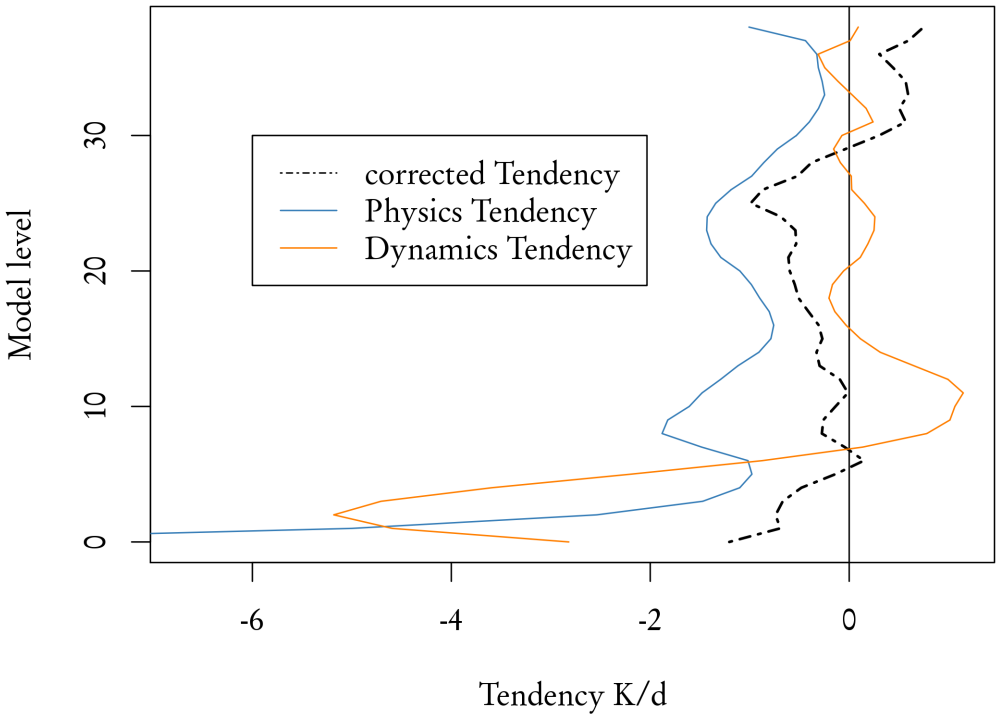

Figure 4.16: *x axis:* Horizontally averaged resulting corrected tendency, physics and dynamics components for the temperature between 12:00 and 18:00 UTC of $\mathrm{K\,d^{-1}}$. Only values north of the tropics are included. *y axis:* Number of the model level.

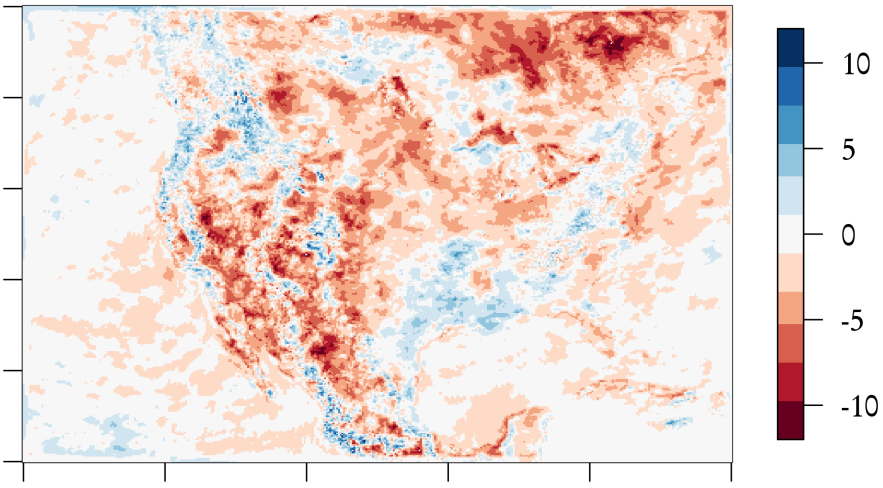

Figure 4.17: *x & y-axis:* Degree North and West, state and country borders are indicated in black lines, state capitals are indicated by black circles *Colors:* The tendency of temperature in the lowest model level between 12:00 and 18:00 UTC in units of $\mathrm{K\,d^{-1}}$

5 Prospects

With the Initial Tendency method different flaws in the forecasts were found. Concentrating not only on build-in prognostic variables, but also adding more easily interpretable variables to the code as well as adding internal components like physics tendencies to the output enabled a successful analysis and explanation of the flaws found.

However this method does only provide additional benefits compared to a classical analysis increment investigation, if computational costs can be reduced by running the model over only one or a few timesteps. The interpretation of these is meaningful only if sufficiently (at least horal) frequent analysis fields are available to correct the background tendencies. If analysis fields are available only less frequently the analysis increment output could be amended by the same physics tendencies and background tendencies resulting in the same product.

Not only subtracting background tendencies but also analyzing them directly proved to be helpful in explaining the flaws found at the upper atmosphere in the WRF model. But the need to redo all forecasts over the whole six hour periods between data assimilation limited the amount of experiments that were affordable. Here it would be conceivable to add key physics parameterizations as well as background tendencies to the standard analysis increment output, allowing for deeper error monitoring in the production system.

In the COSMO model the Initial Tendency method could be deployed more effectively. Here however the early timesteps were dominated by spin-up effects. These can still be considered erroneous but they also exaggerate spin-up effects to dominate the model flaws. This might cover other errors that only become relevant once the model runs for long enough. Here the error found at cloud base in the COSMO model would not have been found, if only the first timesteps were analyzed. Other sources of error like flawed lateral boundary conditions also fall into this category.

Bibliography

Bauer, Peter, Alan Thorpe, and Gilbert Brunet (2015). "The quiet revolution of numerical weather prediction". In: *Nature* 525.7567, pp. 47–55.

Bengtsson, Thomas, Chris Snyder, and Doug Nychka (2003). "Toward a nonlinear ensemble filter for high-dimensional systems". In: *Journal of Geophysical Research: Atmospheres* 108.D24.

Burgers, Gerrit, Peter Jan van Leeuwen, and Geir Evensen (1998). "Analysis scheme in the ensemble Kalman filter". In: *Monthly weather review* 126.6, pp. 1719–1724.

Cavallo, Steven M, Judith Berner, and Chris Snyder (2016). "Diagnosing model errors from time-averaged tendencies in the Weather Research and Forecasting (WRF) Model". In: *Monthly Weather Review* 144.2, pp. 759–779.

Del Genio, Anthony D and Jingbo Wu (2010). "The role of entrainment in the diurnal cycle of continental convection". In: *Journal of Climate* 23.10, pp. 2722–2738.

Doms, G (2011). "Coauthors, 2011: A description of the nonhydrostatic regional COSMO Model. Part II: Physical parameterization". In: *Consortium for Small-Scale Modelling*.

Doms, Günther and M Baldauf (2011). "A Description of the Nonhydrostatic Regional COSMO model. Part I: Dynamics and Numerics". In: *Consortium for Small-Scale Modelling, Deutscher Wetterdienst (DWD)*.

Grandy Jr, WT (2004). "Time evolution in macroscopic systems. II. The entropy". In: *Foundations of Physics* 34.1, pp. 21–57.

Hauf, Thomas and Hartmut Höller (1987). "Entropy and potential temperature". In: *Journal of the atmospheric sciences* 44.20, pp. 2887–2901.

Iacono, Michael J et al. (2008). "Radiative forcing by long-lived greenhouse gases: Calculations with the AER radiative transfer models". In: *Journal of Geophysical Research: Atmospheres* 113.D13.

Janjić, Zaviša I (1994). "The step-mountain eta coordinate model: Further developments of the convection, viscous sublayer, and turbulence closure schemes". In: *Monthly Weather Review* 122.5, pp. 927–945.

– (1996). "The surface layer parameterization in the NCEP Eta Model". In: *World Meteorological Organization-Publications-WMO TD*, pp. 4–16.

– (2001). *Nonsingular implementation of the Mellor-Yamada level 2.5 scheme in the NCEP Meso model*.

Judd, Kevin et al. (2008). "The geometry of model error". In: *Journal of the atmospheric sciences* 65.6, pp. 1749–1772.

Kalman, Rudolph Emil et al. (1960). "A new approach to linear filtering and prediction problems". In: *Journal of basic Engineering* 82.1, pp. 35–45.

Kneifel, Stefan et al. (2012). "Retrospective analysis of regional climate: The German reanalysis project-potential of remote sensing observations". In: *Geoscience and Remote Sensing Symposium (IGARSS), 2012 IEEE International*. IEEE, pp. 3689–3692.

Lambert, JH (1772). *Anmerkungen und Zusätze zur Entwerfung der Himmelscharten. No. 54 in Klassiker ex. Wiss., Engelmann, Leipzig (1894)*.

Laprise, René (1992). "The Euler equations of motion with hydrostatic pressure as an independent variable". In: *Monthly weather review* 120.1, pp. 197–207.

Mlawer, Eli J et al. (1997). "Radiative transfer for inhomogeneous atmospheres: RRTM, a validated correlated-k model for the longwave". In: *Journal of Geophysical Research: Atmospheres* 102.D14, pp. 16663–16682.

Monin, AS and AMF Obukhov (1954). "Basic laws of turbulent mixing in the surface layer of the atmosphere". In:

NCAR (2012). *WRF Public Domain Notice*. URL: `http://www2.mmm.ucar.edu/wrf/users/notice.html` (visited on 04/04/2012).

Paulson, Ca A (1970). "The mathematical representation of wind speed and temperature profiles in the unstable atmospheric surface layer". In: *Journal of Applied Meteorology* 9.6, pp. 857–861.

Remund, Jan, Richard Perez, and Elke Lorenz (2008). "Comparison of solar radiation forecasts for the USA". In: *Proc. of the 23rd European PV Conference*. Vol. 14.

Rodwell, MJ and TN Palmer (2007). "Using numerical weather prediction to assess climate models". In: *Quarterly Journal of the Royal Meteorological Society* 133.622, pp. 129–146.

Schraff, C. and R. Hess (n.d.). "COSMO Documentation Part III: Data Assimilation". In: *Foundations of Physics*.

Schwartz, Craig S et al. (2015). "NCAR's experimental real-time convection-allowing ensemble prediction system". In: *Weather and Forecasting* 30.6, pp. 1645–1654.

Simmer, Clemens et al. (2016). "HErZ: The German Hans-Ertel Centre for Weather Research". In: *Bulletin of the American Meteorological Society* 97.6, pp. 1057–1068.

Skamarock, William C and Joseph B Klemp (2008). "A time-split nonhydrostatic atmospheric model for weather research and forecasting applications". In: *Journal of Computational Physics* 227.7, pp. 3465–3485.

Smith, Leonard A, C Ziehmann, and K Fraedrich (1999). "Uncertainty dynamics and predictability in chaotic systems". In: *Quarterly Journal of the Royal Meteorological Society* 125.560, pp. 2855–2886.

Stephan, Klaus, S Klink, and C Schraff (2008). "Assimilation of radar-derived rain rates into the convective-scale model COSMO-DE at DWD". In: *Quarterly Journal of the Royal Meteorological Society* 134.634, pp. 1315–1326.

Thompson, Gregory et al. (2008). "Explicit forecasts of winter precipitation using an improved bulk microphysics scheme. Part II: Implementation of a new snow parameterization". In: *Monthly Weather Review* 136.12, pp. 5095–5115.

Thornton, Peter E and Nan A Rosenbloom (2005). "Ecosystem model spin-up: Estimating steady state conditions in a coupled terrestrial carbon and nitrogen cycle model". In: *Ecological Modelling* 189.1, pp. 25–48.

Tiedtke, MICHAEL (1989). "A comprehensive mass flux scheme for cumulus parameterization in large-scale models". In: *Monthly Weather Review* 117.8, pp. 1779–1800.

Wahl, Sabrina et al. (2017). “A novel convective-scale regional reanalyses COSMO-REA2: Improving the representation of precipitation”. In: *Meteorol. Z.*

Warner, Thomas T, Ralph A Peterson, and Russell E Treadon (1997). “A tutorial on lateral boundary conditions as a basic and potentially serious limitation to regional numerical weather prediction”. In: *Bulletin of the American Meteorological Society* 78.11, pp. 2599–2617.

Williamson, David L, Jerry G Olson, and Christiane Jablonowski (2009). “Two dynamical core formulation flaws exposed by a baroclinic instability test case”. In: *Monthly Weather Review* 137.2, pp. 790–796.

Zdunkowski, Wilford and Andreas Bott (2003). *Dynamics of the Atmosphere: A course in theoretical Meteorology*. Cambridge University Press.

Zhang, Chunxi, Yuqing Wang, and Kevin Hamilton (2011). “Improved representation of boundary layer clouds over the southeast Pacific in ARW-WRF using a modified Tiedtke cumulus parameterization scheme”. In: *Monthly Weather Review* 139.11, pp. 3489–3513.